eng

Article

Visualization of Movement and Expansion of Coal Reaction Zone by Acoustic Emission Monitoring in Underground Coal Gasification System

Rika Iriguchi [1], Yuma Ishii [1], Akihiro Hamanaka [1,*], Faqiang Su [2], Ken-ichi Itakura [3], Jun-ichi Kodama [4], Takashi Sasaoka [1], Hideki Shimada [1] and Gota Deguchi [5]

1 Department of Earth Resources Engineering, Faculty of Engineering, Kyushu University, Fukuoka 819-0395, Japan; iriguchi.rika.842@s.kyushu-u.ac.jp (R.I.); ishii21r@mine.kyushu-u.ac.jp (Y.I.); sasaoka@mine.kyushu-u.ac.jp (T.S.); shimada@mine.kyushu-u.ac.jp (H.S.)
2 School of Energy Science and Engineering, Henan Polytechnic University, 2001 Century Avenue, Jiaozuo 454003, China; sufq@hpu.edu.cn
3 Endowed Research Laboratory of Un-Mined Mineral Resources and Energy Engineering, Muroran Institute of Technology, Muroran 050-8585, Japan; itakura@mmm.muroran-it.ac.jp
4 Division of Sustainable Resources Engineering, Hokkaido University, Sapporo 060-0808, Japan; kodama@eng.hokudai.ac.jp
5 Mineral Resources Innovation Networks, Non-Profit Organization (NPO), Sapporo 007-0847, Japan; gota@mue.biglobe.ne.jp
* Correspondence: hamanaka@mine.kyushu-u.ac.jp

Citation: Iriguchi, R.; Ishii, Y.; Hamanaka, A.; Su, F.; Itakura, K.-i.; Kodama, J.-i.; Sasaoka, T.; Shimada, H.; Deguchi, G. Visualization of Movement and Expansion of Coal Reaction Zone by Acoustic Emission Monitoring in Underground Coal Gasification System. *Eng* **2023**, *4*, 2960–2977. https://doi.org/10.3390/eng4040166

Academic Editor: Antonio Gil Bravo

Received: 31 October 2023
Revised: 27 November 2023
Accepted: 28 November 2023
Published: 30 November 2023

Abstract: Underground coal gasification (UCG) is the process of directly recovering energy as combustible gases such as hydrogen and carbon monoxide by combusting unmined coal resources in situ. The UCG process is an invisible phenomenon, in which fracturing activity at high temperature (>1000 °C) in coal seams expands the gasification zone and increases the combustible components of the product gas. However, excessive expansion of the gasification zone may cause environmental problems such as gas leakage, deformation of the surrounding ground, and groundwater pollution. Therefore, visualization of the gasification zone of UCG is required for both improving gasification efficiency and developing UCG systems with low environmental impact. In this study, the large-scale model UCG experiments conducted on a laboratory scale (size: 625 mm × 650 mm × 2792 mm (H × W × L)) were carried out to discuss the visualization of the gasification reaction zone of coal in UCG by Acoustic Emission (AE) technique with uniaxial and triaxial acceleration transducers. As the results of temperature monitoring and AE source location analysis show, AE sources are located near the high-temperature zone (>1000 °C). In addition, the located AE sources move and expand with the movement and expansion of the high-temperature zone. AE measurement can be a useful technique for monitoring the progress of the UCG reaction zone. AE measurement with triaxial sensors is also useful to predict a high-temperature zone though the measurable range, which has to be considered.

Keywords: combustion and gasification; gasification control; hydrogen; underground coal gasification; untapped energy

1. Introduction

Underground Coal Gasification (UCG) is a technique of directly recovering energy by converting unmined coal resources in situ into combustible gas. UCG has great potential for effective utilization of previously untapped energy sources because coal has the largest minable reserves of any fossil fuel resources. It is possible to affect the composition of product gas by controlling the gasification agent and the temperature of the coal seam. For example, injecting steam into the combustion zone enhances the production of hydrogen [1,2], and expanding the gasification area with a high temperature enhances gasification reactions, resulting in the production of high-energy gases [3]. Furthermore, UCG is expected to contribute to the reduction in greenhouse gas emissions because the underground coal seam is directly gasified and carbon dioxide can be stored in the large amount of voids formed after gasification [4–6].

The gasification process of UCG is an invisible phenomenon. In UCG, the gasification zone is expanded by fracturing in the coal seam with a high temperature (>1000 °C), which enhances the product gas by accelerating the gasification reaction of UCG over a wide area and the shape and extent of the gasification zone varies with the gasification system [7]. On the other hand, however, since volatile organic compounds are produced as by-products, excessive expansion of the gasification zone causes environmental problems such as gas leakage, deformation of the surrounding ground, and groundwater pollution [8]. For example, in a UCG experiment conducted at Hoe Creek in the United States, targeting coal seams within aquifers at depths of 30–40 m, increased gasification pressure caused surface subsidence and groundwater pollution due to volatile organic compounds [9–11]. Moreover, a previous study has investigated the fracture process as an earthquake prediction tool, considering the similarities between sequences of earthquakes and AE events [12]. Therefore, AE measurement is an important strategy to assist in visualizing the gasification area in UCG for both improving gasification efficiency and developing UCG systems with low environmental impact. AE measurements could be used to monitor the real-time underground coal combustion/gasification area, which would help to reduce unpredictable environmental risks. For example, when sudden gas leakage, deformation of the surrounding ground, and groundwater pollution occur, gasification can be interrupted or the composition of the gasification agency can be changed. This research focuses on the application of acoustic emission (AE) as one of the effective techniques for gasification monitoring because the gasification zone in UCG is expanded by fracturing activities caused by thermal stress around the combustion zone in the coal seam.

Jiang et al. [13] have reported that coal fracture occurs due to the different thermal expansion coefficients of minerals and the expansion of the product gas. In addition, Naka et al. [14] have reported that coal fracture occurs at high temperatures (>500 °C) due to the contraction behavior of coal caused by the bonding and degassing of internal gas bubbles as the softened coal resolidifies to become semi-coke. Many scholars have described that the permeability of coal changes due to rising temperature; the permeability of the coal increases due to the formation of micro fractures at temperatures below 100 °C, the permeability decreases due to thermal expansion at temperatures between 200 °C and 300 °C, and the permeability increases again at temperatures above 300 °C due to the contraction with coal pyrolysis [15–17]. Furthermore, it has been shown that the contraction occurs both in charcoal dust and massive coal [14,18]. The mechanism of micro fractures caused by heating of coal depends on the temperature of the coal. At low temperatures (<300 °C), micro fractures are caused by the expansion pressure of air and steam or by changes in the internal structure due to heating. At high temperatures (300–500 °C), micro fractures are caused by pyrolysis of the coal. AE signal is active especially when the crack width expands under 300–500 °C [19].

In the UCG system, temperatures in the gasification reaction zone are above 1000 °C, and the reaction zone is classified into the oxidation reaction zone (>900 °C), reduction reaction zone (600–900 °C), and pyrolysis zone (300–600 °C) [20,21]. The gasification zone at high temperatures has been estimated by geophysical monitoring such as the resistivity method and seismic tomography [22,23]. In addition, numerical analysis based on the observation results of combustion cavities in coal seams formed by combustion and gasification and data on temperature distribution and heat conduction in coal seams have been used to develop prediction models to estimate the gasification zone formed by UCG and the evolution of the gasification zone [24,25]. The advantage of geophysical monitoring is that it does not require very large measurement equipment, and one- and two-dimensional data can be obtained in a relatively short time from surface-based exploration. On the other hand, its weak point is that the geophysical results obtained may not match the actual underground conditions. Numerical simulation has the advantage of hypothetically simulating underground conditions that cannot actually be observed. Additionally, it can reduce the cost of monitoring. On the other hand, each process of modeling, discretization, and calculation involves a small number of errors. In addition, the calculation process of numerical analysis can require a significant length of time. The AE technique can capture the micro fractures caused by heating of the coal immediately, meaning that it enables establishing real-time monitoring of the gasification zone in the UCG system. Therefore, clarifying that AE monitoring can visualize the movement/expansion of the coal combustion/gasification zone in this study can indicate the possibility of applying AE monitoring to UCG. Moreover, monitoring of fracture activity by using the AE technique contributes to improving gasification efficiency and expanding the gasification area because those should be related to fracturing activities during UCG. Previous UCG model experiments have indicated that many fractures were generated around the gasification reaction zone [3]. Our previous studies have indicated the possibility to utilize the AE technique as a monitoring method of the gasification zone in the UCG system [26]. However, it is still uncertain that the AE technique can visualize the expansion and movement of the gasification reaction zone due to coal combustion/gasification. In addition, the applicability of the AE technique with the triaxial sensors to UCG, which can be installed with less effort and cost by using fewer sensors than uniaxial sensors, is uncertain. In the past experiment, AE could be measured over a wide area in the artificial coal sample by using a large number of uniaxial sensors [3]. However, installing multiple uniaxial sensors underground requires a great effort and cost. On the other hand, triaxial sensors have the potential advantage of being able to estimate the combustion/gasification zone by AE measurement using fewer sensors than uniaxial sensors.

This study discusses the visualization of the gasification reaction zone of coal in UCG by the AE technique by comparing the temperature profiles with AE source location results obtained from large-scale coal seam UCG experiments with the uniaxial sensors and triaxial sensors to UCG.

2. Materials and Methods

2.1. Acoustic Emission (AE)

AE measurement systems differ in the type of sensor used, the AE signal processing system, the material to be measured, and the measuring environment. Figure 1 shows the AE measurement system used in this study. The sensor which receives the AE signals is an acceleration transducer (620HT; Teac Corp., Tokyo, Japan), which is compatible with high temperatures. The AE signals received in an acceleration transducer are recorded in a high-speed multi-recorder (GR-7000; Keyence Corp., Osaka, Japan) after they are transmitted to an amplifier (SA-611; Teac Corp.) by a low-noise cable. In the amplifier, the high-pass filter is set at 5 Hz and the low-pass filter is set at 10,000 Hz to filter out noise in the signals. In the high-speed multi-recorders, edge triggering is applied to record the AE signals when the input AE signal exceeds the threshold, and OR triggering is applied when several acceleration transducers are used. The threshold is set at 0.1 m/s^2. The sampling time interval is 2 μs with a record length of 2500 records and a pre-trigger of 20%.

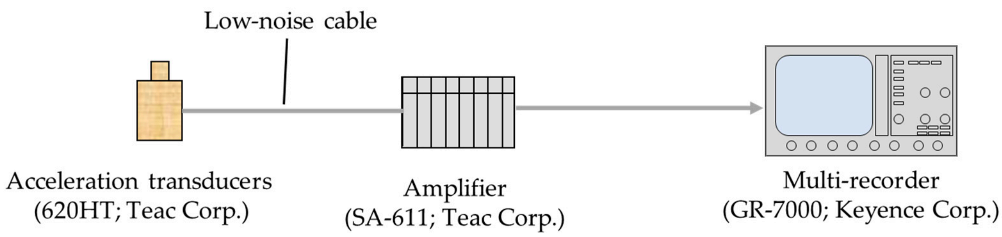

Figure 1. AE measurement system.

In AE source location analysis using several uniaxial sensors, the Akaike Information Criterion (AIC) is applied to the threshold AE waveform data as a method of calculating arrival time of the threshold AE waveform [27]. The most probable location of the AE source is calculated by the iterative least squares method, which uses arrival time of the threshold AE waveform to the acceleration transducer, the coordinate of the acceleration transducers, and the velocity of elastic waves propagating through the sample by programming in Visual Studio 2010 [28]. Also, VRML ver2.0 is used for visualization of AE source location. In AE source location analysis using several triaxial sensors, the arrival time of the P-wave is calculated by AIC and that of S-wave is calculated by threshold. The direction of fracturing source is determined from P-wave direction calculated by the least squares method. In addition, the AE source location is calculated from the difference between the P-wave and S-wave in arrival times and propagation velocities.

2.2. Large-Scale UCG Model Experiment

In this study, large-scale UCG model experiments are conducted using artificial coal seam samples. Figure 2 shows a setup of the UCG experiment using an artificial coal seam sample. In the experiments, the coal seam sample was prepared by pouring a mixture of 1.2 tons of crushed coal, cement, and water at a ratio of 10:0.5:1 (by weight) into a steel container with internal dimension of 625 mm × 650 mm × 2792 mm (H × W × L). Heat-resistant concrete is injected above the coal block to reduce gas leakage. Coal is collected from the Sunago Coal Mine in Hokkaido, Japan. Table 1 shows the proximate and ultimate analysis of the coal sample used in the experiments. Figure 3 shows top and side view of the artificial coal seam sample of Experiments 1 and 2. A co-axial well with a length of 2600 mm and a diameter of 90 mm is installed at the bottom of the artificial coal seam sample. Different designs were adopted in Experiments 1 and 2; only a horizontal well was adopted in Experiment 1 and a horizontal well with an auxiliary production well was adopted in Experiment 2. In experiment 2, an auxiliary well with a length of 2600 mm and a diameter of 40 mm is installed at the top of the artificial coal seam sample. To the author's knowledge, an auxiliary production well has never been applied in previous UCG model experiments. The method of the UCG experiment is the horizontal co-axial method, which collects the UCG gas produced around the combustion zone from between the injection pipe and the co-axial well.

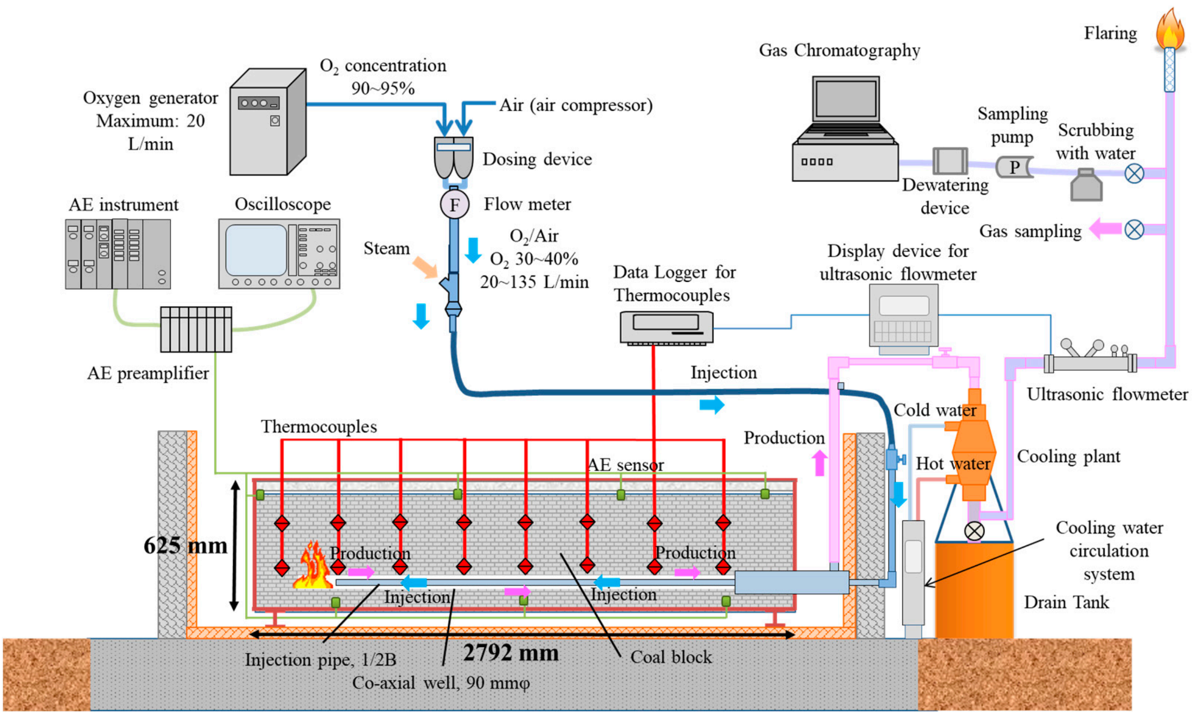

Figure 2. Experimental setup of the large-scale UCG experiment.

Table 1. Proximate and ultimate analysis of coal.

	Calorific Value (MJ/kg)	Proximate Analysis (wt%)				Ultimate Analysis (wt%)				
		Moisture	Ash	Volatiles	Fixed Carbon	C	H	N	S	O
Experiment 1	24.4	4.2	22.2	34.0	39.6	61.5	4.46	1.28	-	9.54
Experiment 2	24.6	4.7	20.7	33.5	41.1	62.4	4.55	1.27	0.04	10.0

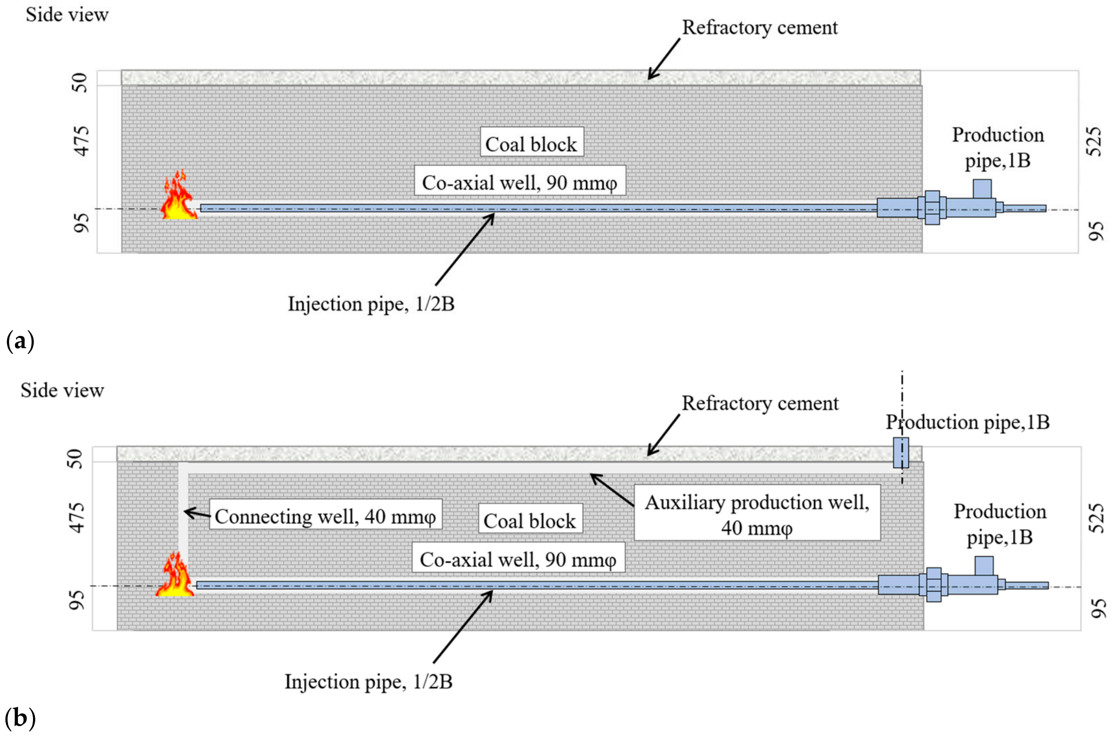

Figure 3. Side view of artificial coal seam samples: (**a**) Experiment 1; (**b**) Experiment 2.

Figure 4 shows the arrangement of thermocouples (1SKF613, 1SKF615; CHINO Corp., Tokyo, Japan). To measure temperature changes in the sample, thermocouples compatible with high temperature are installed into the coal from the top and side of the coal seam sample. The thermocouples are fixed by a gypsum aqueous solution. The vertical positions of the thermocouples are T11 to T18 directly above the co-axial well, T21 to T28 150 mm above the co-axial well, and T31 to T38 300 mm above the co-axial well. T41 to T44 are placed at different heights from the side of the coal seam sample in order to measure temperature change deeper than the bottom of the co-axial well.

Figure 5 shows the arrangement of AE sensors. We install acceleration transducers as sensors to capture the AE signals generated from the combustion coal. The purpose of this attempt is to monitor the expansion of the coal combustion/gasification zone and the progress of fractures in that zone. The acceleration transducers are attached to the coal sample by stainless steel waveguides of 6 mm in diameter and 100 mm in length. The holes with 35 mm in diameter and with 50 mm in length for the waveguides were drilled from the surface of a steel container to the coal sample. The waveguides are fixed by a mixture of gypsum and cement. Ten uniaxial acceleration transducers (620HT; Teac Corp.) are installed on the sides of the coal seam sample and two triaxial acceleration transducers (731ZT; Teac Corp.) are installed inside the artificial coal seam sample as shown in Figure 5 (AE3-1 and AE3-2).

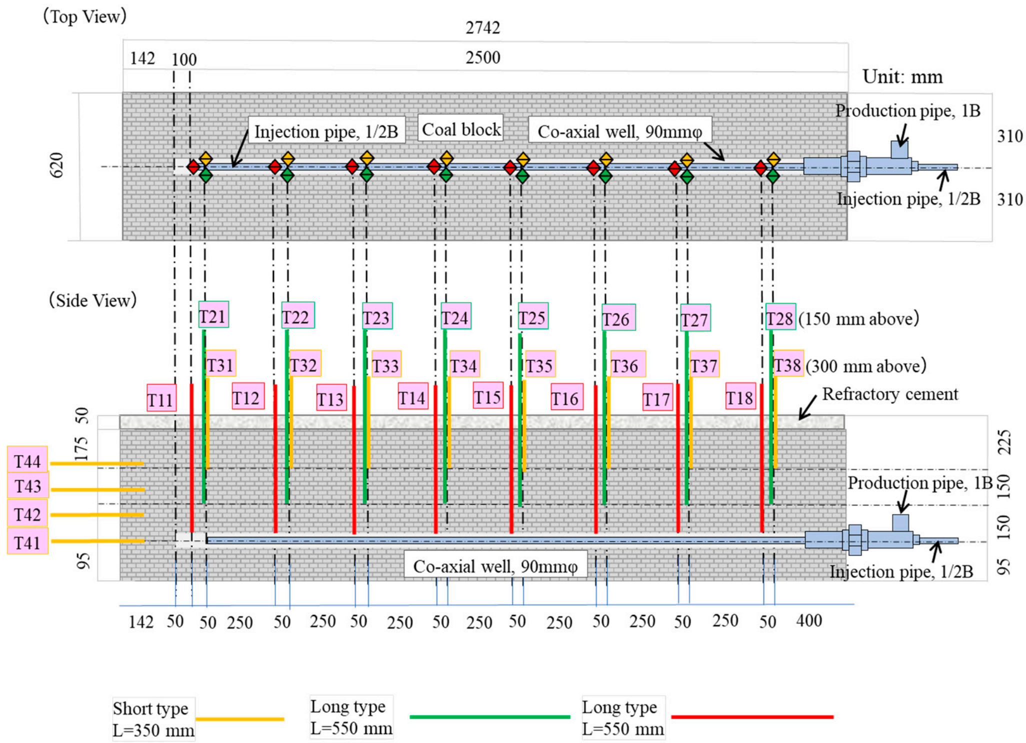

Figure 4. Distribution of thermocouples.

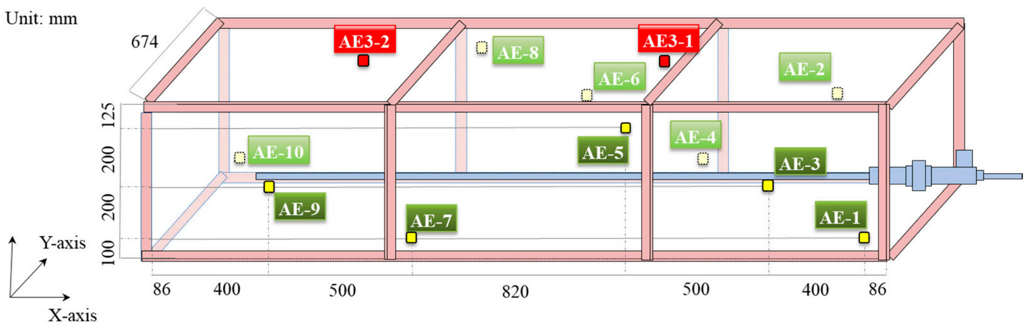

Figure 5. Distribution of acceleration transducers.

The coal was ignited by supplying oxygen-enriched air (oxygen concentration: 34%) and propane gas from the injection pipe while the nichrome wire attached to the tip of the injection pipe was energized. After the ignition of coal was successful, a gasification agency consisting of air and oxygen (oxygen concentration: 33.3%) was continuously injected to maintain gasification of the coal sample during the experiments. The gasification agency flow rate was sequentially increased from 35 L/min (oxygen flow rate: 12.1 L/min) to a maximum of 120 L/min (oxygen flow rate: 40 L/min) while monitoring the carbon monoxide, carbon dioxide, and hydrogen concentrations in the product gas. After the start of the experiment, the injection pipe inserted in the co-axial well was sequentially pulled out by 300 mm, expecting that the combustion/gasification zone would move to the unreacted coal area. The experimental durations for Experiments 1 and 2 are 91 and 81 h, respectively.

3. Results and Discussion

This study discusses the visualization of the coal gasification reaction zone in UCG by AE measurements and examines the applicability of uniaxial and triaxial sensors to UCG by comparing temperature profiles and AE source location results. In this study, "Step" was defined based on changes in the tip location of the injection pipe and the flow rate of the gasification agency when comparing AE source location results with the temperature profiles. Table 2 shows the definition of each Step in Experiments 1 and 2 based on the distance from the bottom of the co-axial well to the injection pipe tip and the injection flow rate of the gasification agency.

Table 2. Definition of each Step in Experiments 1 and 2.

Experiment 1			**Experiment 2 (with Auxiliary Production Well)**		
Step	**Time (h)**	**Injection Location (mm)**	**Step**	**Time (h)**	**Injection Locatione (mm)**
1~5	1~17	150~350	1~5	1~13	100~300
6~10	17~46	350~800	6~10	13~31	300~500
11~15	46~71	800~1300	11~15	31~56	500~900
16~20	71~91	1300~1800	16~20	56~81	900~1400

Figures 6 and 7 show the temperature profile recorded by thermocouples, the coal cross section after the experiment, and the gasification zone in Experiments 1 and 2. The range of temperature profile is from 200 °C to 1200 °C. The coal cross section is a vertical cross section of the artificial coal seam. The photographs of the coal cross section are taken by cutting vertically every 100 mm of the coal seam sample. The gypsum solution is poured into the coal seam after the experiment. The cross section photographs of coal are divided into the combustion/gasification zone (cavity), ash-deposited combustion/gasification zone (ash) coal char gasification zone (char), pyrolysis zone (pyrolysis), and unreacted zone (coal, black). Figure 7 shows that Experiment 2 (with auxiliary production well) expands the high-temperature zone (1000 °C) and the reacted zone of coal including cavities, ash, char, and pyrolysis after gasification compared to Experiment 1 without the auxiliary production well. Moreover, the coal cross section in Figure 7b also shows that the combustion/gasification zone expands to the top of the coal sample. Therefore, these results indicate that the combustion/gasification zone is expanded to the top of the coal sample by installing an auxiliary production well in addition to the co-axial well in the coal seam of the UCG system.

3.1. AE Source Location Analysis by Uniaxial Sensors

Figures 8 and 9 show the temperature profiles and the results of uniaxial AE source location for each Step in Experiments 1 and 2, respectively. The red sphere indicates the location of the AE source, and the yellow sphere indicates the location of the center of gravity of all AE sources. The center of gravity of the AE sources indicates the location where the AE sources are concentrated. The temperature monitoring area in the results of uniaxial AE source location is indicated by a dashed line. AE sources are located near the high-temperature zone above 1000 °C. This indicates that AE is caused by fracture activity in the coal seam in the high-temperature zone above 1000 °C. In Figures 8 and 9, AE sources are also observed in the 200 °C and 600 °C temperature zone. Although the reason for this is uncertain, it could be caused by expansion pressure of air and steam or by changes in the internal structure due to heating, or by pyrolysis of coal [19]. The location of the high-temperature zone, AE sources, and center of gravity of the AE sources moves horizontally from the bottom side of the co-axial well to the injection/production side with elapsed time. It is also observed that AE sources are distributed throughout the coal sample.

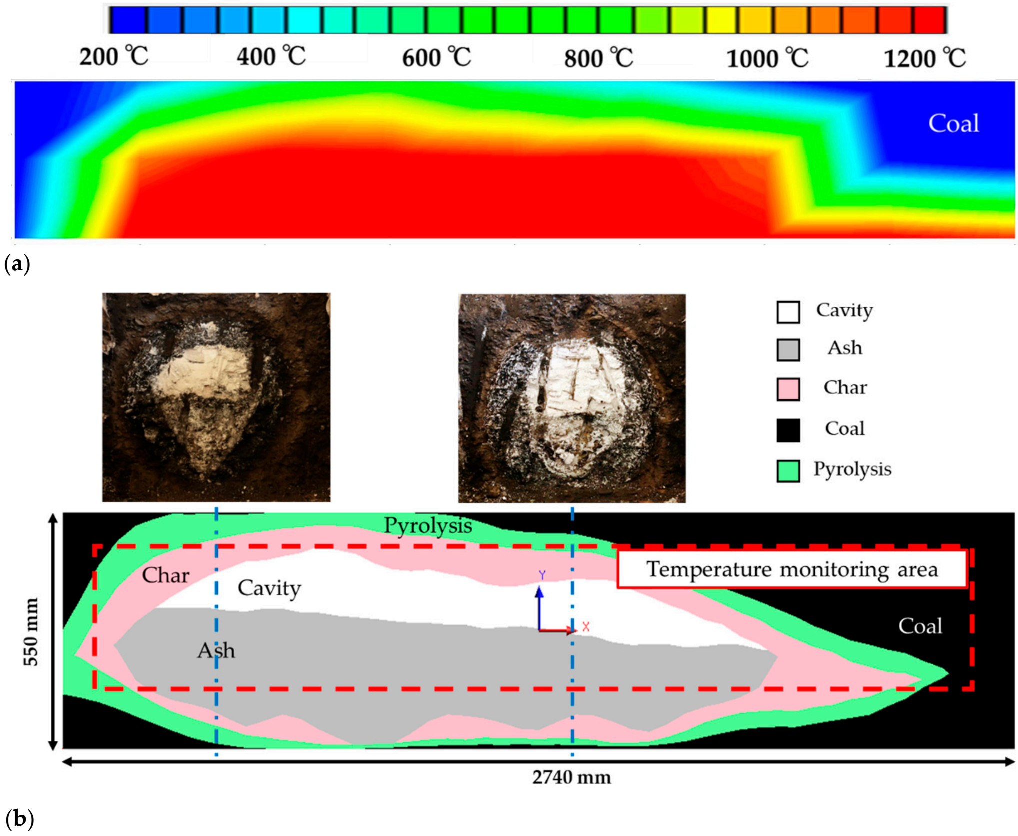

Figure 6. Results of Experiment 1: (**a**) temperature profile; (**b**) coal cross section and gasification zone.

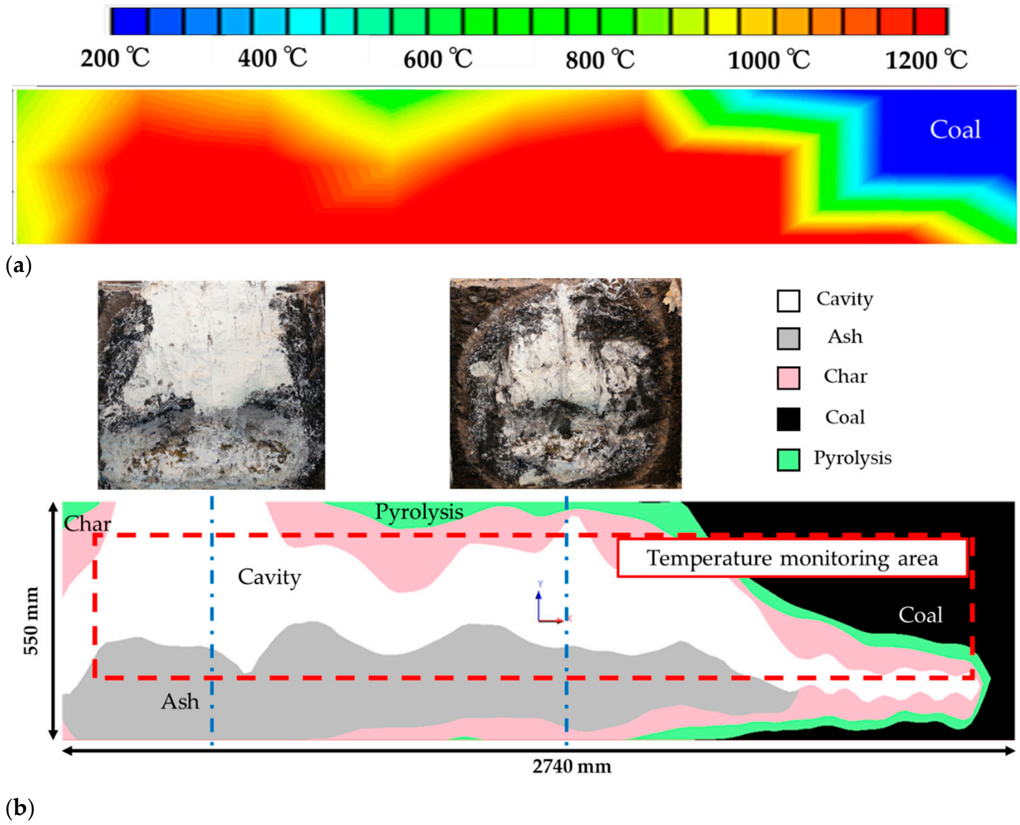

Figure 7. Results of Experiment 2: (**a**) temperature profile; (**b**) coal cross section and gasification zone.

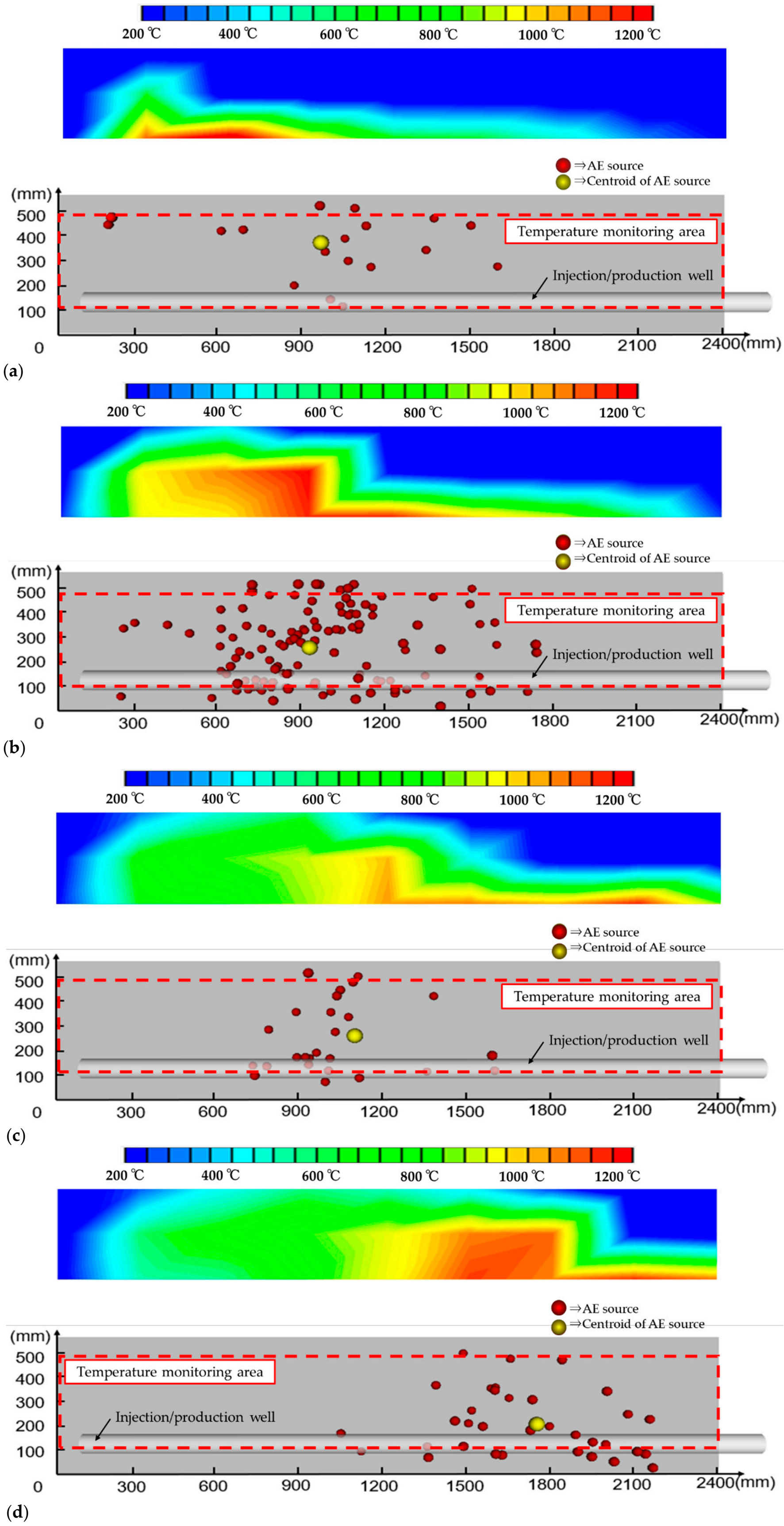

Figure 8. Uniaxial AE source location in Experiment 1: (**a**) Steps 1~5; (**b**) Steps 6~10; (**c**) Steps 11~15; (**d**) Steps 16~20.

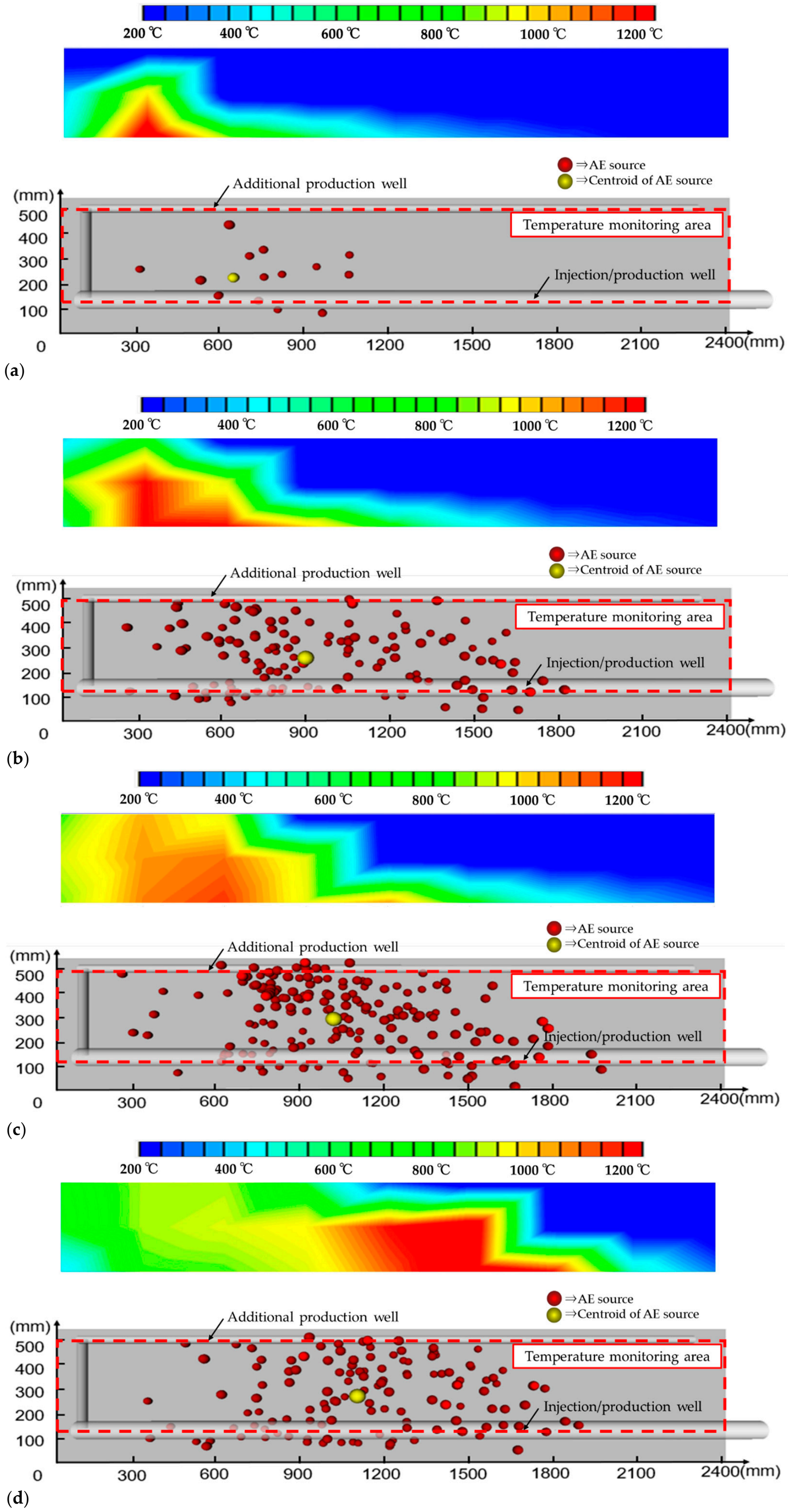

Figure 9. Uniaxial AE source location in Experiment 2: (**a**) Steps 1~5; (**b**) Steps 6~10; (**c**) Steps 11~15; (**d**) Steps 16~20.

Tables 3 and 4 show the horizontal movement rate of the center of gravity of the AE sources. The movement rate is calculated by dividing the horizontal moved distance by the movement time of the center of gravity. Table 3 shows that in Experiment 1 (without auxiliary production well), the horizontal movement rates of the center of gravity of the AE sources are 115 mm/h, −1.11 mm/h, 5.56 mm/h, and 28.9 mm/h for Steps 1~5, 6~10, 11~15, and 16~20, respectively. Table 4 shows that in Experiment 2 (with auxiliary production well), the horizontal movement rates of the center of gravity of the AE sources are 100 mm/h, 20.0 mm/h, 2.91 mm/h, and 4.00 mm/h for Steps 1~5, 6~10, 11~15, and 16~20, respectively. Tables 5 and 6 show the horizontal movement rate of the temperature zone above 1000 °C. In UCG, the gasification zone expands as a result of fracturing in the coal seam under high-temperature conditions (above 1000 °C); therefore, it is important to consider the horizontal movement rate in the high-temperature zone above 1000 °C. Furthermore, although coal fracturing activity is reported to occur at temperatures below 1000 °C, temperatures below 1000 °C are located immediately around the temperature zone above 1000 °C [20]. Therefore, the horizontal movement rate of the temperature zone below 1000 °C was considered to be the same as that of the temperature zone above 1000 °C. The movement rate is calculated by dividing the movement distance of each temperature by the movement time. The horizontal movement distance for each temperature is equal to the horizontal distance of the thermocouple at which each temperature was observed. Table 5 shows that in Experiment 1 (without auxiliary production well), the horizontal movement rates of the temperature zone above 1000 °C are 41.2 mm/h, 15.6 mm/h, 42.6 mm/h, and 13.3 mm/h for Steps 1~5, 6~10, 11~15, and 16~20, respectively. Table 6 shows that in Experiment 2 (with auxiliary production well), the horizontal movement rates of the temperature zone above 1000 °C are 7.69 mm/h, 20.0 mm/h, 14.0 mm/h, and 24.0 mm/h for Steps 1~5, 6~10, 11~15, and 16~20, respectively. Tables 3 and 4 show that in Steps 1~5, the horizontal movement rate of the center of gravity of Experiment 1 (without auxiliary production well) is 115 mm/h, which is 14.7 mm/h higher than that of Experiment 2 (with auxiliary production well). In Tables 5 and 6, a similar trend is observed in the movement rate of the temperature zone above 1000 °C. In Tables 5 and 6, the horizontal movement rate in the temperature zone above 1000 °C is 41.2 mm/h in Experiment 1 (without auxiliary production well), which is 33.5 mm/h higher than that of Experiment 2 (with auxiliary production well). Although the values of the horizontal movement rate of the center of gravity of the AE sources and the horizontal movement rate of the temperature zone above 1000 °C are different in both experiments, the trends of the horizontal movement rate of the AE sources and of the high-temperature zone are captured. Table 3 shows that the horizontal movement rate of the center of gravity of the AE sources increases 6.67 mm/h from Steps 6~10 to Steps 11~15 in Experiment 1 (without auxiliary production well). Additionally, Table 5 shows that the horizontal movement rate of the temperature zone above 1000 °C increases 27 mm/h from Steps 6~10 to Steps 11~15 in Experiment 1 (without auxiliary production well). On the other hand, Table 4 shows that the horizontal movement rate of the center of gravity of the AE sources decreases 17.1 mm/h from Steps 6~10 to Steps 11~15 in Experiment 2 (with auxiliary production well) and Table 6 shows that the horizontal movement rate of the temperature zone above 1000 °C decreases 6.05 mm/h from Steps 6~10 to Steps 11~15 in Experiment 2 (with auxiliary production well). Although the values of the horizontal movement rate of the center of gravity of the AE sources and the horizontal movement rate of the temperature zone above 1000 °C are different in both experiments, the trends of the horizontal movement rate of the AE sources and of the high-temperature zone are captured in Steps 6~10 and Steps 11~15. These results indicate that the center of gravity of the AE sources moves more quickly toward the injection/production side in Experiment 1 (without auxiliary production well) than in Experiment 2 (with auxiliary production well). This is considered to be an effect of the expansion of the combustion/gasification zone of the coal sample to the upper part of the coal seam sample rather than horizontally, due to installing the auxiliary production well in the upper part of the coal seam sample in Experiment 2. For example, comparing the number of AE sources located above 400 mm from the bottom in Figures 8c and 9c, the number of AE sources in Experiment 2 is larger than in Experiment 1. Furthermore, the temperature profile in Figure 9c shows that the high-temperature zone above 1000 °C is located more than 200 mm above that found in Figure 8c. These results suggest that the AE source location with uniaxial acceleration transducers can visualize the movement/expansion of the combustion/gasification reaction zone of the UCG. Therefore, it is possible to visualize the movement/expansion of the coal combustion reaction zone by uniaxial AE acceleration transducer, and it is revealed that uniaxial AE source location can be a useful technique for monitoring the progression of the UCG reaction zone.

Table 3. Horizontal movement rate of the center of gravity of AE sources in Experiment 1.

Experiment 1 (without Auxiliary Production Well)	**Step 0**	**Steps 1~5**	**Steps 6~10**	**Steps 11~15**	**Steps 16~20**
Location of center of gravity (mm)	0.0	975.0	950.0	1100.0	1750.0
Start time (h)	0	1	17	46	71
End time (h)	1	17	46	71	91
Intermediate time (h)	0.5	9	31.5	58.5	81
Movement rate (mm/h)	-	115	−1.11	5.56	28.9

Table 4. Horizontal movement rate of the center of gravity of AE sources in Experiment 2.

Experiment 2 (with Auxiliary Production Well)	**Step 0**	**Steps 1~5**	**Steps 6~10**	**Steps 11~15**	**Steps 16~20**
Location of center of gravity (mm)	0.0	650.0	950.0	1012.5	1112.5
Start time (h)	0	1	13	31	56
End time (h)	1	13	31	56	81
Intermediate time (h)	0.5	7	22	43.5	68.5
Movement rate (mm/h)	-	100	20.0	2.91	4.00

Table 5. Horizontal movement rate of the temperature zone above 1000 °C in Experiment 1.

Experiment 1 (without Auxiliary Production Well)	**Step 0**	**Steps 1~5**	**Steps 6~10**	**Steps 11~15**	**Steps 16~20**
Location of temperature range above 1000 °C (mm)	0.0	350.0	700.0	1850.0	2150.0
Start time (h)	0	1	17	46	71
End time (h)	1	17	46	71	91
Intermediate time (h)	0.5	9	31.5	58.5	81
Movement rate (mm/h)	-	41.2	15.6	42.6	13.3

Table 6. Horizontal movement rate of the temperature zone above 1000 °C in Experiment 2.

Experiment 2 (with Auxiliary Production Well)	**Step 0**	**Steps 1~5**	**Steps 6~10**	**Steps 11~15**	**Steps 16~20**
Location of temperature range above 1000 °C (mm)	0.0	50.0	350.0	650.0	1250.0
Start time (h)	0	1	13	31	56
End time (h)	1	13	31	56	81
Intermediate time (h)	0.5	7	22	43.5	68.5
Movement rate (mm/h)	-	7.69	20.0	14.0	24.0

Figure 10 shows the principle of the AE profile. The purpose of the AE profile is to discuss the distribution of AE sources which occurred in Experiments 1 and 2. The coal sample is divided vertically into three sections with 150 mm at the bottom and 200 mm at the middle and top, and horizontally into 13 sections with 210 mm at both edges and 200 mm between them. The number of AE sources in each section ranges from 0 to 20 units. Figure 11 shows the AE profiles for each Step in Experiments 1 and 2, respectively. In Figure 11c,d, the distribution of AE sources expands widely to the top of the coal seam sample in Experiment 2 after Step 10. This is considered to be an effect of the expansion of the combustion/gasification zone of the coal sample to the upper part of the coal seam sample rather than horizontally, due to installing the auxiliary production well in the upper part of the coal seam sample in Experiment 2. This result shows a similar trend in the results for the coal cross section, temperature profile, and uniaxial AE source location. In Steps 1~5, it is considered that the AE sources may not be successfully detected depending on the distribution of the AE acceleration transducer because the high-temperature zone is relatively small in the early stages of gasification. Therefore, it is revealed that AE profiles can be used to monitor the movement of the coal combustion/gasification zone.

Figure 10. Principle of AE profile.

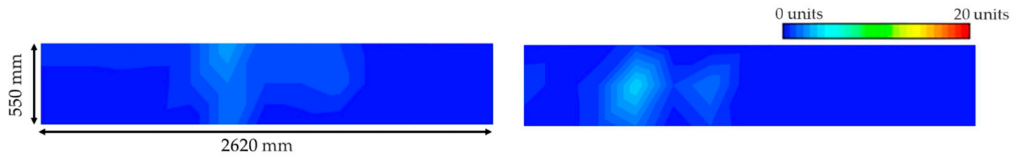

(**a**) Steps 1~5 of Experiments 1 and 2.

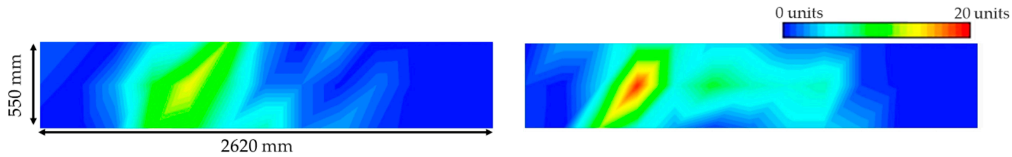

(**b**) Steps 6~10 of Experiments 1 and 2.

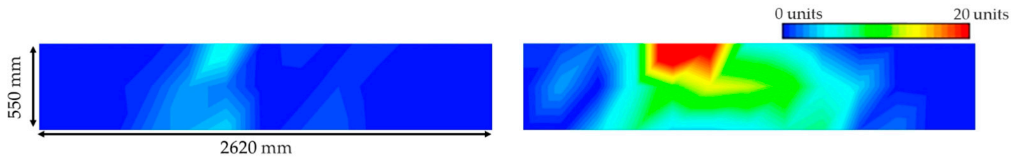

(**c**) Steps 11~15 of Experiments 1 and 2.

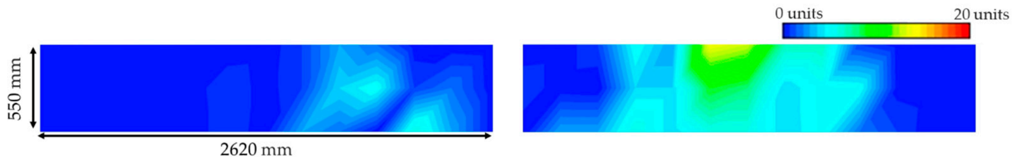

(**d**) Steps 16~20 of Experiments 1 and 2.

Figure 11. Results of AE profile.

3.2. AE Source Location Analysis by Triaxial Sensor

The results of AE source location using the uniaxial acceleration transducers confirm the possibility of visualizing the gasification zone related to the movement/expansion of the combustion/gasification zone in the artificial coal seam sample. However, since many uniaxial acceleration transducers are required, the triaxial AE measurement with less sensors can be considered as a more useful monitoring technology than the uniaxial AE measurement.

Figure 12 shows the temperature profiles and the results of triaxial AE source location for each Step in Experiment 2. The yellow sphere shows the location of the triaxial acceleration transducers (AE3-1 and AE3-2), and the red sphere shows the location of the AE source. The temperature monitoring area in the results of triaxial AE source location is marked as a dashed line. The AE sources are located near the high-temperature zone above 1000 °C. Comparing Figure 12a,b, the number of AE sources increases and the AE source area observed in AE3-2 expands when the high-temperature zone expands in temperature profiles. The result is due to a chain of expanding combustion/gasification zones. The combustion/gasification zone of the coal further expands as the temperature in the coal seam sample increases and a large number of AEs are generated due to the thermal contraction behavior of the coal [14]. Furthermore, the result can also be explained by the expansion of the coal combustion/gasification zone and the generation of a large number of fracturing activities in a larger area around AE3-2 by moving the ignition point from the bottom side of the co-axial well to the injection/production side with the progress of the Step. In Figure 12c,d, as the high-temperature zone above 1000 °C moves horizontally from the bottom side of the co-axial well to the injection/production side with the progress of the Step, the AE source location also tends to move horizontally as well. Although it is a subject for future work to clarify the movement rate of the AE source observed by the triaxial acceleration transducer, the horizontal movement of the AE source is clearly recognized from Figure 12c,d, associated with the horizontal movement of the high-temperature zone above 1000 °C. In other words, AE source location by using triaxial acceleration transducers shows almost the same trend as the results of uniaxial source location, indicating that it is possible to visualize the movement/expansion of the combustion/gasification zone during UCG with less triaxial sensors. In the uniaxial source location, the AE source is distributed throughout the coal sample, while in the triaxial source location in Figure 12, the range of the AE source location observed in AE3-2 is distributed only around its acceleration transducers. Additionally, in Figure 12d, the results of the AE source observed in AE3-1 show a similar trend as AE3-2. Installing multiple uniaxial sensors underground requires a great effort and cost; on the other hand, triaxial sensors have the potential advantage of being able to estimate the combustion/gasification zone by AE measurement using fewer sensors than uniaxial sensors. However, the area of AE observed is relatively localized in triaxial acceleration transducers, meaning that the measurable area of the triaxial acceleration transducers is relatively limited compared to that of uniaxial acceleration transducers. This is due to the fact that in triaxial AE source location, AE events cannot be detected due to wave attenuation if the distance from the fracturing source to the single acceleration transducer is far [12]. Although the range of AE source location is limited to the area around the sensor compared to multiple uniaxial sensors, we consider that source location by triaxial sensors is still sufficient to estimate the high-temperature area, considering the disadvantage of uniaxial sensors. Therefore, triaxial AE source location requires us to consider the location of the sensor to detect AE events and the measurable range in advance. In the future, assuming field-scale UCG, it is necessary to develop a visualization technique for the underground coal combustion/gasification area by triaxial AE source location, considering the measurable area. The exiting accelerations have potential applications in the real world, but we have not yet found out if we can measure AE in the real field by using them. We need to confirm this on a field-scale test in the future. Specifically, it is necessary to confirm whether the existing accelerations can measure small fracture activity caused by temperature changes in coal in a field-scale UCG experiment. In other words, if the accelerations are installed in a well for environmental measurement, it is necessary to examine what distance between the gasification reaction zone and the accelerations is sufficient for AE measurement in the case of a field-scale UCG system. Future studies are expected to accumulate the data from large-scale UCG experiments and examine the complex geological and hydrological conditions of the subsurface.

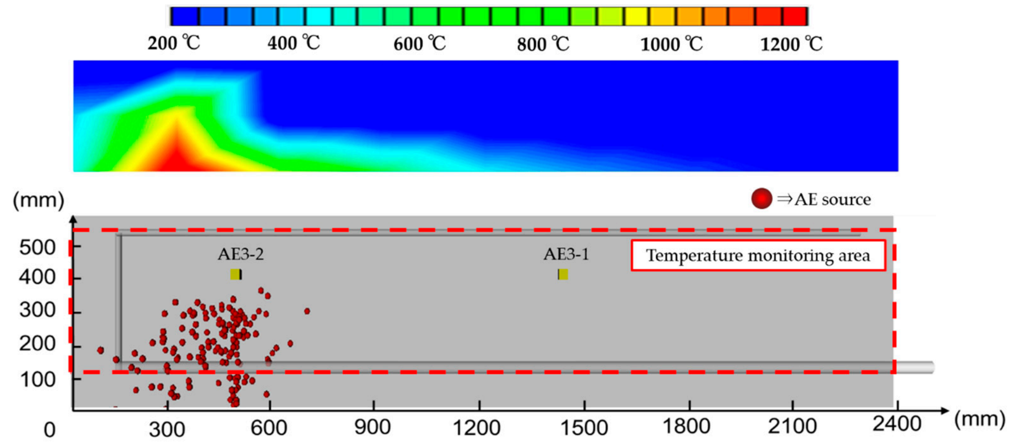

(**a**) AE3-2 in Step 5.

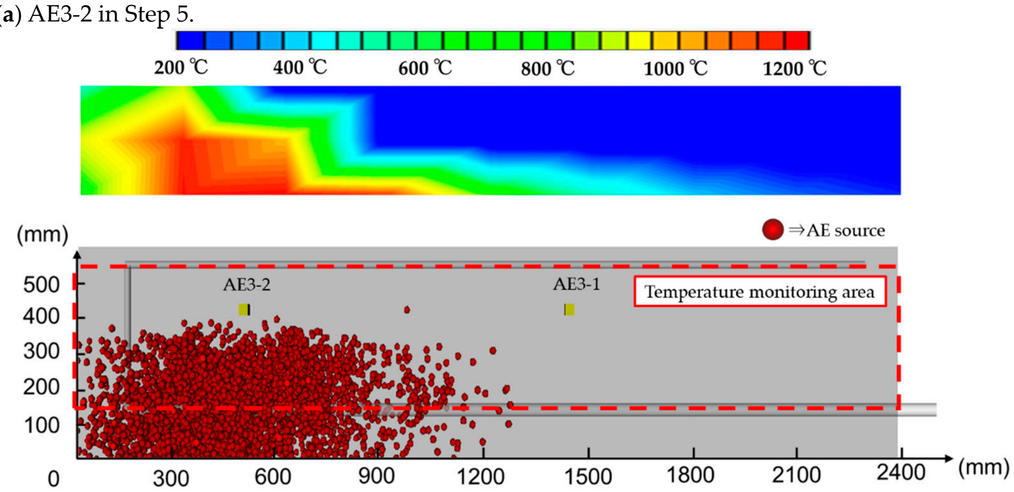

(**b**) AE3-2 in Step 11.

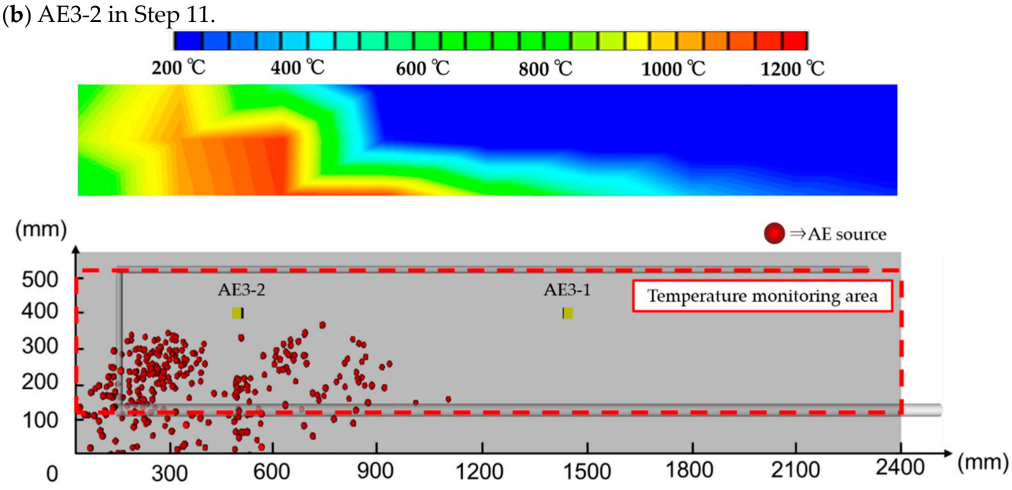

(**c**) AE3-2 in Step 13.

Figure 12. *Cont.*

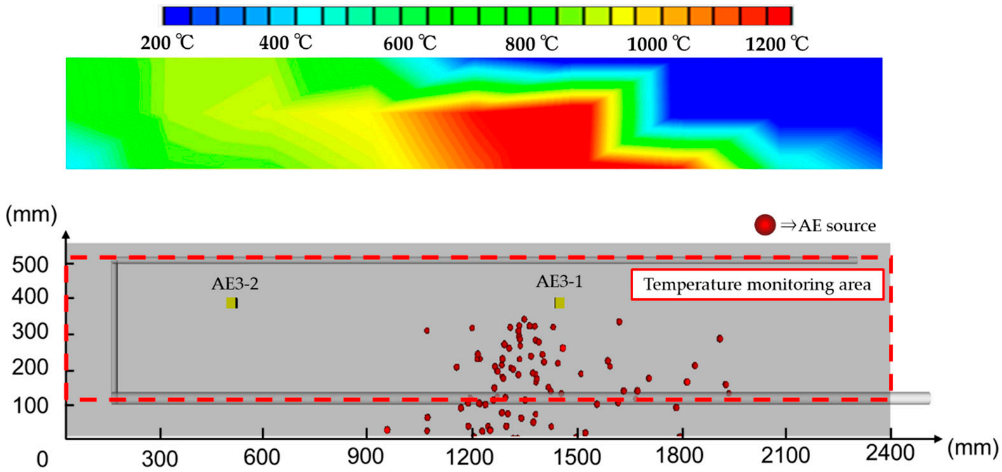

(**d**) AE3-1 in Step 20.

Figure 12. Triaxial AE source location in Experiment 2: (**a**) Step 5; (**b**) Step 11; (**c**) Step 13; (**d**) Step 20.

4. Conclusions

This study investigates the applicability of the AE technique as a system of monitoring progression in the coal gasification zone during UCG through the large-scale UCG experiment. We have obtained the following knowledge.

- The AE sources are located near the high-temperature zone above 1000 °C.
- The results of AE source location are comparable with the temperature profile; as the high-temperature zone moves and expands, the AE sources that occur around the combustion/gasification zone move and expand.
- AE profiles can be used to monitor the expansion of the coal combustion/gasification zone.
- In triaxial AE source location, the area of AE observed is limited to the area around its acceleration transducer.
- The uniaxial and triaxial AE source location can be a useful technique for monitoring the progress of the UCG reaction zone.
- It is necessary to consider the measurable range of a few triaxial acceleration transducers when applying triaxial AE source location to UCG.
- In the future, assuming a field-scale UCG system, it is necessary to develop a visualization technique for the underground coal combustion/gasification area by triaxial AE source localization, considering the measurable area of triaxial acceleration transducers.

Author Contributions: Conceptualization, R.I., A.H. and K.-i.I.; methodology, Y.I. and G.D.; software (Visual Studio 2010 and VRML ver2.0), R.I., Y.I. and A.H.; validation, T.S.; formal analysis, H.S.; investigation, J.-i.K.; resources, F.S.; data curation, G.D.; writing—original draft preparation, R.I.; writing—review and editing, A.H. and H.S.; visualization, Y.I.; supervision, K.-i.I. and J.-i.K.; project administration, K.-i.I. All authors have read and agreed to the published version of the manuscript.

Funding: This work was supported by Mikasa City, the Japanese Society on UCG, Kyushu University Platform of Inter-/Transdisciplinary Energy Research (Q-PIT) through its “Module-Research Program”, JSPS KAKENHI Grant Number JP21K14575 and JP22K05005.

Institutional Review Board Statement: Not applicable.

Informed Consent Statement: Not applicable.

Data Availability Statement: Data will be available on request.

Acknowledgments: The authors gratefully acknowledge the support of UCG project members and express particular appreciation to them.

Conflicts of Interest: The authors declare no conflict of interest.

References

1. Yang, L.H.; Zhang, X.; Liu, S.Q.; Yu, L.; Zhang, W.L. Field test of large-scale hydrogen manufacturing from underground coal gasification (UCG). *Int. J. Hydrogen Energy* **2008**, *33*, 1275–1285. [CrossRef]
2. Liu, S.Q.; Wang, Y.Y.; Zhao, K.; Yang, N. Enhanced-hydrogen gas production through underground gasification of lignite. *Min. Sci. Technol.* **2009**, *19*, 389–394. [CrossRef]
3. Hamanaka, A.; Su, F.Q.; Itakura, K.; Takahashi, K.; Kodama, J.; Deguchi, G. Effect of Injection Flow Rate on Product Gas Quality in Underground Coal Gasification (UCG) Based on Laboratory Scale Experiment: Development of Co-Axial UCG System. *Energies* **2017**, *10*, 11. [CrossRef]
4. Burchart-Korol, D.; Krawczyk, P.; Czaplicka-Kolarz, K.; Smolinski, A. Eco-efficiency of underground coal gasification (UCG) for electricity production. *Fuel* **2016**, *173*, 239–246. [CrossRef]
5. Yang, D.M.; Koukouzas, N.; Green, M.; Sheng, Y. Recent development on underground coal gasification and subsequent CO_2 storage. *J. Energy Inst.* **2016**, *89*, 469–484. [CrossRef]
6. Khadse, A.; Qayyumi, M.; Mahajam, S.; Aghalayam, P. Underground coal gasification: A new clean coal utilization technique for India. *Energy* **2007**, *32*, 2061–2071. [CrossRef]
7. Lozynskyi, V. Critical review of methods for intensifying the gas generation process in the reaction channel during underground coal gasification (UCG). *Min. Miner. Depos.* **2023**, *17*, 67–85. [CrossRef]
8. Bhutto, A.W.; Bazmi, A.A.; Zahedi, G. Underground coal gasification: From fundamentals to applications. *Prog. Energy Combust. Sci.* **2013**, *39*, 189–214. [CrossRef]
9. Wang, F.T.; Mead, S.W.; Stuermer, D.H. (Eds.) *Groundwater Contamination Near the Hoe Creek UCG Experiments*; Lawrence Livermore National Lab.: Livermore, CA, USA, 1981.
10. Wang, F.T.; Mead, S.W.; Stuermer, D.H. (Eds.) *Mechanisms for Groundwater Contamination by UCG—Preliminary Conclusions from the Hoe Creek Study*; Sandia National Laboratories (Technical Report) SAND: Albuquerque, NM, USA, 1982.
11. Perkins, G. Underground coal gasification—Part I: Field demonstrations and process performance. *Prog. Energy Combust. Sci.* **2018**, *67*, 158–187. [CrossRef]
12. Lockner, D. The role of acoustic emission in the study of rock fracture. In *International Journal of Rock Mechanics and Mining Sciences & Geomechanics Abstracts*; Pergamon: Bergama, Turkey, 1993; Volume 30, pp. 883–899.
13. Jiang, C.; Wang, Y.; Duan, M.; Guo, X.; Chen, Y.; Yang, Y. Experimental study on the evolution of pore-fracture structures and mechanism of permeability enhancement in coal under cyclic thermal shock. *Fuel* **2021**, *304*, 121455. [CrossRef]
14. Naka, R.; Tatekawa, T.; Kodama, J.I.; Sugawara, T.; Itakura, K.I.; Hamanaka, A.; Deguchi, G. (Eds.) Thermal stress analysis on small-scale model experiment for development of underground coal gasification. In Proceedings of the ISRM International Symposium—10th Asian Rock Mechanics Symposium, Singapore, 29 October–3 November 2018; ARMS: Waltham, MA, USA, 2018.
15. Kasani, H.A.; Chalaturnyk, R.J. Influence of High Pressure and Temperature on the Mechanical Behavior and Permeability of a Fractured Coal. *Energies* **2017**, *10*, 854. [CrossRef]
16. Yangsheng, Z.; Fang, Q.; Zhijun, W.; Yuan, Z.; Weiguo, L.; Qiaorong, M. Experimental investigation on correlation between permeability variation and pore structure during coal pyrolysis. *Transp. Porous Media* **2010**, *82*, 401–412. [CrossRef]
17. Liu, S.Q.; Zhang, S.J.; Chen, F.; Wang, C.H.; Liu, M.Y. Variation of Coal Permeability under Dehydrating and Heating: A Case Study of Ulanqab Lignite for Underground Coal Gasification. *Energy Fuels* **2014**, *28*, 6869–6876. [CrossRef]
18. Matsudaira, K.; Nishimura, M.; Asada, S. Control of breaking strength of CO_2 reacted coke by crushing operation of coal. *Curr. Adv. Mater. Process.* **1998**, *11*, 843.
19. Ding, R.; Sun, Q.; Xue, S.Z.; Shi, Q.M.; Ge, Z.L.; Li, D.L. Experimental study on acoustic emission characteristics of high-temperature thermal damage in an oxygen-rich environment of long flame coal. *J. Therm. Anal. Calorim.* **2022**, *147*, 11391–11400. [CrossRef]
20. Wang, Z.Q.; Xu, X.Y.; Cui, Y. Effect of Fixed and Removable Gas-Injection Patterns on the Expansion of Reaction Zones during Underground Coal Gasification. *Energy Fuels* **2019**, *33*, 4740–4747. [CrossRef]
21. Wang, Z.Q.; Liang, J.; Shi, L.X.; Xi, J.F.; Li, S.; Cui, Y. Expansion of three reaction zones during underground coal gasification with free and percolation channels. *Fuel* **2017**, *190*, 435–443. [CrossRef]
22. Tatiana, S.; Igor, G.; Alexey, B. Control of combustion area using electrical resistivity method for underground coal gasification. *Int. J. Min. Sci. Technol.* **2012**, *22*, 351–355.
23. Mellors, R.; Yang, X.; White, J.A.; Ramirez, A.; Wagoner, J.; Camp, D.W. Advanced geophysical underground coal gasification monitoring. *Mitig. Adapt Strateg. Glob Chang.* **2016**, *21*, 487–500. [CrossRef]
24. Perkins, G. Underground coal gasification—Part II: Fundamental phenomena and modeling. *Prog. Energy Combust. Sci.* **2018**, *67*, 234–274. [CrossRef]
25. Samdani, G.; Aghalayam, P.; Ganesh, A.; Sapru, R.K.; Lohar, B.L.; Mahajani, S. A process model for underground coal gasification—Part-I: Cavity growth. *Fuel* **2016**, *181*, 690–703. [CrossRef]
26. Su, F.Q.; Wu, J.B.; Deng, Q.C.; Yu, Y.H.; Hamanaka, A.; Dai, M.J.; Yang, J.N.; He, X.L. Study on the monitoring method of cavity growth in underground coal gasification under laboratory conditions. *Energy* **2023**, *263*, 126048. [CrossRef]

27. Ohno, K.; Shimozono, Y.; Sawada, Y.; Ohtsu, M. Automatic Detection of AE First Mortion Based on AIC Picker for SiGMA Analysis. *J. Jpn. Soc. Non-Destr. Insp.* **2008**, *57*, 531–536.
28. Hardy, H.R. *Acoustic Emission/Microseismic Activity Volume 1*, 1st ed.; CRC Press: London, UK, 2003.